Biogeosciences, 9, 3917–3930, 2012
www.biogeosciences.net/9/3917/2012/
doi:10.5194/bg-9-3917-2012

Biogeosciences

High temporal and spatial variability of dissolved oxygen and pH in a nearshore California kelp forest

C. A. Frieder[1], **S. H. Nam**[2], **T. R. Martz**[3], **and L. A. Levin**[1,4]

[1]Integrative Oceanography Division, Scripps Institution of Oceanography, University of California San Diego, 9500 Gilman Drive, 92093–0218 La Jolla, CA, USA
[2]Climate, Atmospheric Science and Physical Oceanography, Scripps Institution of Oceanography, University of California San Diego, 9500 Gilman Drive, 92093–0230 La Jolla, CA, USA
[3]Geosciences Research Division, Scripps Institution of Oceanography, University of California San Diego, 9500 Gilman Drive, 92093–0244 La Jolla, CA, USA
[4]Center for Marine Biodiversity and Conservation, Scripps Institution of Oceanography, University of California San Diego, 9500 Gilman Drive, 92093–0218 La Jolla, CA, USA

Correspondence to: C. A. Frieder (ctanner@ucsd.edu)

Received: 13 March 2012 – Published in Biogeosciences Discuss.: 30 March 2012
Revised: 30 August 2012 – Accepted: 10 September 2012 – Published: 12 October 2012

Abstract. Predicting consequences of ocean deoxygenation and ocean acidification for nearshore marine ecosystems requires baseline dissolved oxygen (DO) and carbonate chemistry data that are both high-frequency and high-quality. Such data allow accurate assessment of environmental variability and present-day organism exposure regimes. In this study, scales of DO and pH variability were characterized over one year in a nearshore kelp forest ecosystem in the Southern California Bight. DO and pH were strongly, positively correlated, revealing that organisms on this upwelling shelf are not only exposed to low pH but also to low DO. The dominant scale of temporal DO and pH variability occurred on semi-diurnal, diurnal and event (days–weeks) time scales. Daily ranges in DO and pH at 7 m water depth (13 mab) could be as large as 220 µmol kg^{-1} and 0.36 units, respectively. Sources of pH and DO variation include photosynthesis within the kelp forest ecosystem, which can elevate DO and pH by up to 60 µmol kg^{-1} and 0.1 units over one week following the intrusion of high-density, nutrient-rich water. Accordingly, highly productive macrophyte-based ecosystems could serve as deoxygenation and acidification refugia by acting to elevate DO and pH relative to surrounding waters. DO and pH exhibited greater spatial variation over a 10 m increase in water depth (from 7 to 17 m) than along a 5 km stretch of shelf in a cross-shore or alongshore direction. Over a three-month time period, mean DO and pH at 17 m water depth were 168 µmol kg^{-1} and 7.87, respectively. These values represent a 35 % decrease in mean DO and 37 % increase in [H^+] relative to near-surface waters. High-frequency variation was also reduced at depth. The mean daily range in DO and pH was 39 % and 37 % less, respectively, at 17 m water depth relative to 7 m. As a consequence, the exposure history of an organism is largely a function of its depth of occurrence within the kelp forest. With knowledge of local alkalinity conditions and high-frequency temperature, salinity, and pH data, we estimated pCO_2 and calcium carbonate saturation states with respect to calcite and aragonite (Ω_{calc} and Ω_{arag}) for the La Jolla kelp forest at 7 m and 17 m water depth. pCO_2 ranged from 246 to 1016 µatm, Ω_{calc} was always supersaturated, and Ω_{arag} was undersaturated at the beginning of March for five days when pH was less than 7.75 and DO was less than 115 µmol kg^{-1}. These findings raise the possibility that the benthic communities along eastern boundary current systems are currently acclimatized and adapted to natural, variable, and low DO and pH. Still, future exposure of coastal California populations to even lower DO and pH may increase as upwelling intensifies and hypoxic boundaries shoal, compressing habitats and challenging the physiological capacity of intolerant species.

Published by Copernicus Publications on behalf of the European Geosciences Union.

1 Introduction

Increased levels of atmospheric carbon dioxide (CO_2) have reduced subsurface oxygen concentrations and increased acidity of surface waters (Gruber, 2011; Doney et al., 2012). Ocean deoxygenation is due to a combination of warming, increased stratification and altered ocean circulation (Keeling et al., 2010). Ocean acidification is an increase in oceanic CO_2 uptake and the concomitant decrease in seawater pH and saturation states of calcium carbonate (Ω; Doney et al., 2009). Much of what has been learned about carbonate chemistry and dissolved oxygen (DO) trends and trajectories in the ocean is based upon open-ocean conditions measured via ship-based hydrographic time series that sample quarterly, annually or even less often. This limits our understanding of DO and carbonate chemistry dynamics in nearshore settings.

The coastal environment is a highly variable system. Fluctuations in temperature, salinity, air–sea gas exchange, mixing processes and biogeochemical processes can have large influences on DO and pH. There are contemporary nearshore environments, particularly eastern boundary current systems, which are exposed to low pH, high pCO_2, and low Ω conditions during upwelling events (Feely et al., 2008; Hofmann et al., 2011b). Deoxygenation and acidification are of particular concern in tandem in ocean regions where DO and inorganic carbon are tightly linked through local primary production and/or remineralization of organic matter (Cai et al., 2011; Gruber, 2011; Hofmann et al., 2011a). Understanding the nature and drivers of DO and carbonate chemistry dynamics along eastern boundary current systems, which harbor ecologically and economically important species, will provide insight into the relative sensitivity of these systems to a changing ocean climate.

There has been much emphasis on understanding the physical characteristics of nearshore waters in upwelling systems, and different scales of variability have been identified and associated with specific processes. Sources of variability in temperature and nutrients, for example, include El Niño-Southern Oscillation (ENSO), seasonal and temporal upwelling, coastally trapped waves, coastal sea breeze, and internal tidal waves and bores (Pineda, 1999; Lerczak et al., 2001; Lluch-Cota et al., 2001; Kaplan et al., 2003; Pringle and Riser, 2003), but there is presently limited information regarding DO and pH dynamics in relation to these different scales of variability. Recent studies have found that the upper horizon of the hypoxic boundary (defined as $60\,\mu mol\,kg^{-1}$) in the Southern California Bight (SCB) has shoaled by almost 100 m near the coastline since the 1980s (Bograd et al., 2008), with consequences for benthic fishes (McClatchie et al., 2010). ENSO cycles also influence DO over the SCB shelf. The 2010 La Niña event led to a 38–50 % decline in DO relative to the normal seasonal mean (Nam et al., 2011). Strong upwelling events also bring low pH water toward the surface along the eastern Pacific margin, with pH_{sws} values falling below 7.7 near the coastline (Feely et al., 2008). Some high-frequency variability in pH has been reported in nearshore habitats (Hofmann et al., 2011b; Yu et al., 2011; Booth et al., 2012). Results indicate that pH signatures are ecosystem and site-specific with characteristic diel, semidiurnal, and stochastic patterns of varying amplitudes. Kelp forests in upwelling regions can exhibit large fluctuations in pH conditions due to a combination of mixing, tidal excursions, upwelling, and biological activity (Hofmann et al., 2011b).

The SCB is characterized by water masses from the subarctic and tropical Pacific through the California Current and California Undercurrent (Bray et al., 1999; Dong et al., 2009). Seasonal upwelling is strongest during the spring when equatorward currents lift isopycnal surfaces and bring low DO and low pH water from intermediate depths onto the continental shelf (Bray et al., 1999; Feely et al., 2008). The complex bathymetry and coastline of the SCB drives extensive variability in circulation features, and coastal regions are affected by both locally and coastally propagated remote forcing that drives temporal upwelling events at timescales of a few days to weeks (Pringle and Riser, 2003; Dong et al., 2009; Send and Nam, 2012). The SCB also harbors one of the world's fastest growing primary producers, the giant kelp *Macrocystis pyrifera*. Kelp forests are abundant along the SCB coast (North et al., 1993), and serve as the foundation for diverse and energy-rich habitats of great ecological and economic importance (Graham et al., 2007). Understanding the DO and pH dynamics within kelp forests will provide detailed information regarding the corresponding exposure histories for a diversity of valued species of molluscs, echinoderms, crustaceans and fishes. Additionally, it is important to identify present-day carbonate chemistry conditions in coastal macrophyte-dominated ecosystems, as recent evidence suggests that under high-CO_2 scenarios kelps have variable but often positive responses to elevated CO_2 (Swanson and Fox, 2007; Roleda et al., 2012). A working hypothesis for kelps in the SCB is that they may respond positively to the direct and indirect effects of ocean acidification but negatively to the direct and indirect effects of warming (Harley et al., 2012). Still, other evidence suggests that under high-CO_2 scenarios canopy-forming macroalgae could experience greater competition with noncalcareous turf species (Connell and Russell, 2010; Hepburn et al., 2011).

Here, we characterize variability of DO and pH in the La Jolla kelp forest (LJKF) and adjacent nearshore settings. We deployed two sensors in a variety of configurations in order to ask the following questions: What are the dominant short-term scales of pH and DO variability? Is there spatial variation in pH and DO within the kelp forest linked to depth, alongshore direction, or cross-shore direction? What is the relationship between pH and DO in the kelp forest and is the relationship stable in time and space? To constrain the carbonate system in nearshore settings, two of the four possible parameters must be directly measured or estimated with robust empirical relationships (Cullison Gray et al., 2011; Alin

et al., 2012). With knowledge of local alkalinity conditions and the high-frequency pH, salinity and temperature data, we estimated pCO_2 and Ω for two forms of $CaCO_3$, calcite and aragonite (Ω_{calc} and Ω_{arag}, respectively), and consider how spatial and temporal heterogeneity in carbonate chemistry and DO may influence different levels of biological organization and organism exposure histories.

2 Methods

2.1 Field measurements

We used moorings deployed on the inner shelf, located within and around the LJKF to explore cross-shore, alongshore and water depth effects on DO and pH between July 2010 and November 2011 (Fig. 1). The shelf in this region is 8 km wide and the kelp forest, at its fullest extent, is 8 km long and up to 1.5 km wide. Time-series data were collected with a sampling rate of 15 min using two instruments placed in different configurations among moorings (Fig. 1). Data were nearly continuously collected from mooring A (32.81° N 117.29° W; 20 m bottom depth) within the LJKF. The sensor was attached 13 m above bottom (mab or 7 m water depth) to explore variability in DO and pH over multiple temporal scales (Fig. 1a). Changes in DO and pH with water depth were investigated by comparing concurrent data from mooring A at 7 m and 17 m (3 mab) below the surface (Fig. 1b). Alongshore changes in DO and pH were explored by comparing sensor data from 7 m water depth from mooring A and mooring D (32.85° N 117.28° W; 20 m bottom depth), which was located 5 km to the north in an alongshore direction and still within the LJKF (Fig. 1c). Cross-shore changes in DO and pH were explored by comparing sensor data from 7 m water depth at different locations along an east–west transect perpendicular to the local coastline (Fig. 1d). In 2010, the paired moorings were mooring B, 3.5 km from the coast (32.81° N 117.31° W; 30 m bottom depth), and mooring A, 1.9 km from the coast. Mooring B is located offshore of the kelp forest. In 2011, the paired moorings were mooring A (1.9 km from the coast) and mooring C, 1.4 km from the coast (32.81° N 117.28° W; 15 m bottom depth). Concurrent DO and pH data exist for all deployments except that no pH data were available from August to November 2011 at mooring A due to a sensor malfunction.

Data were collected using two "SeapHOx" instrument packages. The SeapHOx consists of a Honeywell Durafet III pH sensor (Martz et al., 2010), an Aanderaa 3835 oxygen optode, and an SBE-37 MicroCAT CTD. One of the MicroCAT CTDs was equipped with a pressure sensor. We compared LJKF data with current speed and direction measured in the upper 30 m of the water column (100 m bottom depth) from the Del Mar mooring located 14 km to the NW (DM Buoy: 32.94° N 117.32° W). Current data were obtained every 7.5 min at 5 m intervals from 5 to 100 m using

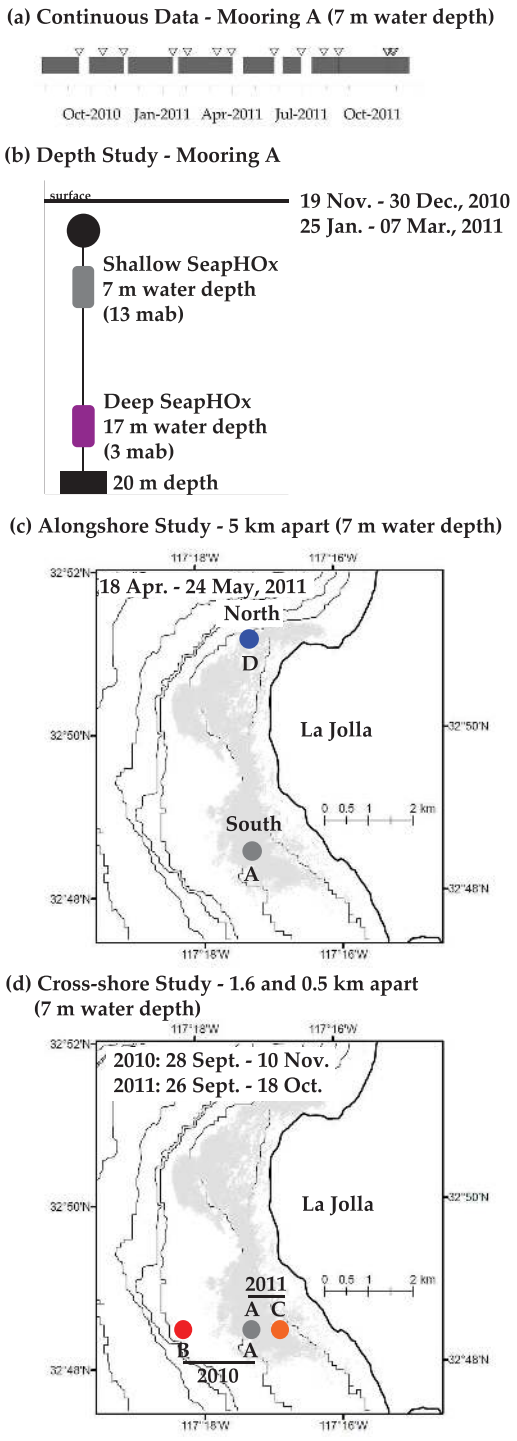

Fig. 1. Placement of SeapHOx sensors among moorings to characterize DO and pH differences **(a)** over time, **(b)** with depth, **(c)** in an alongshore direction, and **(d)** in a cross-shore direction. Bathymetric contours are in 10 m increments (10–60 m depth). At least one discrete sample (upside-down triangles) was taken per SeapHOx deployment to calibrate the pH sensor. Color scheme of moorings corresponds with subsequent figures. Grey shading in **(c)** and **(d)** depicts maximum extent of the La Jolla Kelp Forest based on aerial surveys from 1989–2009 (California Department of Fish and Game).

a down-looking 300 kHz acoustic Doppler current profiler (ADCP).

2.2 Calibrations

To calibrate the pH sensors, discrete water samples were taken during each SeapHOx deployment for the determination of total alkalinity (TA) and total dissolved inorganic carbon (DIC) (Fig. 1a). The calibration samples were collected via SCUBA next to the sensor with a 5 l Niskin bottle during the middle and/or end of the sensor deployment. This was not done at the beginning of the deployment because we found the pH sensor requires a day before providing stabilized data. The collected seawater was transferred to a 500 ml clean borosilicate glass bottle with a ground glass neck and stopper. The samples were poisoned with a saturated mercuric chloride solution. TA measurements were determined using an open-cell, potentiometric titration (Dickson et al., 2007). DIC measurements were determined by acid extraction and coulometric detection of CO_2 (Dickson et al., 2007). pH was calculated from TA and DIC using the Matlab version of CO2SYS (van Heuven et al., 2011) with dissociation constants from Mehrbach et al. (1973) as refitted by Dickson and Millero (1987). The calculated pH at in situ temperature from the calibration sample was used to determine the electrode-specific calibration coefficients. When two calibration samples were taken during the same SeapHOx deployment, they were averaged since we did not find significant evidence of drift and these sensors have been shown to be stable for months at a time (Martz et al., 2010). The calibration sample produced a pH accuracy of 0.01 units for each SeapHOx instrument. The oxygen sensors were factory calibrated by Aanderaa, and before each deployment a two-point (0 % and 100 % saturation) offset was applied as recommended in the manual. Data from SeapHOx deployments presented in this paper are available at http://osprey.bco-dmo.org.

2.3 Data analysis

DO and pH data from the SeapHOx sensors were analyzed as either unfiltered data in order to illustrate the extremes and rates of change or a 2-d running mean was applied to raw data. pH is reported on the total hydrogen ion scale at in situ temperature. Extreme salinity outliers (≥ 3 SD) were removed, and density was calculated from salinity and temperature data. Time in all figures is shown in Coordinated Universal Time (UTC). Although uptake and release of dissolved inorganic carbon leads to a slightly nonlinear relationship between pH and DO, for the purposes of our statistical description a simple linear fit between the two was sufficient to distinguish underlying patterns, and the use of higher-order functions was deemed unnecessary. Accordingly, the relationship between DO and pH was determined with a Model-II least squares fit for all concurrent data of DO and pH. Spectral analyses were calculated on detrended datasets using a fast fourier transform. Spectra of temperature, DO and pH were averaged over four 16-d windows from the longest continuous deployment at mooring A, 7 m below the surface from 25 January 2011–31 March 2011. Pressure data were not available during this time period. Instead, spectra were averaged over four 11.5-d windows from 29 July 2010–13 September 2010, and averaging yielded a typical power spectrum of pressure for this region. To explore DO, pH, and temperature cycles at semidiurnal and diurnal timescales, a fast fourier transform was applied to data and desired frequencies were bandpass filtered (e.g., $DO_{f=1}$ or $DO_{f=2}$, frequency of once per day or twice per day). Current data obtained from the DM mooring were decomposed into cross-shore (u) and alongshore (v) components, and both were smoothed with a 2-d running mean. Equatorward phases were designated as time periods when the alongshore current velocity at all depths between 5 and 30 m was southward, e.g., $v < 0$, and poleward phases were designated as time periods when alongshore current velocity at all depths between 5 and 30 m was northward, e.g., $v > 0$.

pCO_2, Ω_{arag}, and Ω_{calc} were estimated from the high-frequency pH, temperature, and salinity data generated by the SeapHOx at 7 m and 17 m water depth at mooring A, along with upper and lower estimates of TA for the LJKF. The lower and upper values chosen for TA were 2225 and 2260 µmol kg^{-1}. These values are 5 µmol kg^{-1} beyond that observed from the minimum and maximum values from all discrete samples ($n = 18$) taken for SeapHOx calibration purposes. Additionally, these values fall within the range reported by Alin et al. (2012) for TA < 100 m water depth. Carbonate chemistry parameters were calculated using the Matlab version of CO2SYS (van Heuven et al., 2011). Using the upper and lower limit of TA for this system along with pH, temperature and salinity data resulted in an average range for each calculated value of pCO_2 of 8 µatm. The average ranges for each calculated value of Ω were 0.031 for Ω_{arag} and 0.049 for Ω_{calc}.

3 Results

3.1 Temporal variability in dissolved oxygen and pH

3.1.1 Diurnal and semidiurnal scales of dissolved oxygen and pH variability

Two time scales of periodic variability were identified within one year at mooring A: semidiurnal and diurnal. The average daily range (peak-to-peak) in DO and pH were 63 µmol O_2 kg^{-1} ($n = 249$ d; SD = 39.4) and 0.11 pH units ($n = 169$ d; SD = 0.07). The daily range could be as great as 220 µmol O_2 kg^{-1} and 0.36 pH units. DO, pH, temperature and pressure at 7 m water depth exhibited energetic variance at both the semidiurnal and diurnal frequencies (Fig. 2). Semidiurnal variance was greater than diurnal

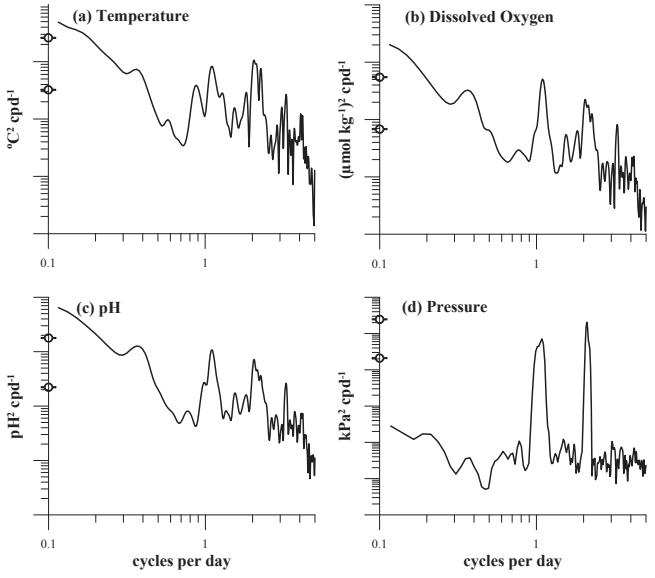

Fig. 2. Frequency power spectra (cycles per day) from mooring A at 7 m water depth for **(a)** temperature, **(b)** dissolved oxygen, **(c)** pH and **(d)** pressure. The circles on the left side of each graph denote the critical scale for 95 % confidence in energy peaks.

variance for temperature and pressure, but diurnal variance was greater than semidiurnal variance for DO and pH. Semidiurnal and diurnal DO and pH fluctuations had differing proportions of physical and biological forcing. Semidiurnal fluctuations in DO and pH were well correlated with temperature, suggesting that the primary source of semidiurnal variability was physical isothermal fluctuations ($DO_{f=2} = 19.2 \times temp_{f=2}$, $R^2 = 0.85$, $P < 0.001$; $pH_{f=2} = 0.03 \times temp_{f=2}$, $R^2 = 0.74$, $P < 0.001$). DO and pH were less correlated with temperature at the diurnal band ($DO_{f=1} = 16.4 \times temp_{f=1}$, $R^2 = 0.55$, $P < 0.001$; $pH_{f=1} = 0.03 \times temp_{f=1}$, $R^2 = 0.53$, $P < 0.001$). A decrease in correlation at the diurnal bandwidth indicates that diurnal isothermal fluctuations either play less of a role in diurnal forcing of DO and pH, or other mechanisms (e.g., diel scales of production and respiration, and/or air–sea gas exchange associated with diurnal land–sea breeze) are opposing diurnal modulations in DO and pH forced by temperature. These observed high-frequency scales of fluctuations in the LJKF are not only persistent through time, but also encompass a large range of DO and pH conditions.

3.1.2 Event-scale variability in dissolved oxygen and pH

Overall increases and decreases in DO and pH, and intermittent amplifications of higher-frequency (e.g., diurnal and semidiurnal) fluctuations lasting from days to weeks, were observed in the LJKF. Here we define changes in pH and DO lasting more than one day to multiple weeks as event-scale variability.

Mean increases in DO and pH: Notable increases in DO and pH were observed for approximately a week following the occasional intrusion of high-density (deep, cold, and nutrient-rich) water. High-density waters were defined as $\sigma > 25.1\,kg\,m^{-3}$. This value has been suggested to reflect water containing the threshold concentration of nitrate required for kelp growth (Parnell et al., 2010). During 2010–2011 there were seven events (observed among all moorings) when high-density seawater shoaled to 7 m water depth (Table 1). These events fueled primary production and increased DO and pH with the exception of the August 2010 event at mooring B, when high mean DO ($290\,\mu mol\,kg^{-1}$) existed prior to the intrusion of high-density seawater. ΔDO and ΔpH were calculated as the difference between the mean value for seven days before the intrusion of high-density seawater and the mean value for seven days after the intrusion of high-density seawater. The magnitude of the regional water velocity after the event (v after) explained 62 % of the variation in ΔpH ($\Delta pH = 0.012 \times v$ after $- 0.02$, $R^2 = 0.62$, $P = 0.035$). The greatest ΔDO and ΔpH values occurred when alongshore currents transitioned from equatorward to strong poleward currents. As an illustrative example, such an event occurred during late April to early May 2011 at mooring D (Fig. 3). Mean DO at $\sigma < 25.1$ prior to the event was $247\,\mu mol\,kg^{-1}$, and mean DO at $\sigma < 25.1$ the subsequent week was $309\,\mu mol\,kg^{-1}$, reflecting a 20 % increase in DO. The corresponding mean pH before and after the event was 8.07 and 8.17, respectively. Similar observations were made during the same time period in south LJKF (mooring A). Mean DO before the event was $249\,\mu mol\,kg^{-1}$, and mean DO after the event was $312\,\mu mol\,kg^{-1}$. The corresponding mean pH before and after the event at mooring A was 8.05 and 8.15, respectively. The influx of high-density, nutrient-replete water masses occurred when alongshore current direction was equatorward and was followed by a strong poleward reversal that stimulated biological production within the LJKF, causing a release of DO, uptake of CO_2, and thus increased pH.

Mean decreases in DO and pH: Event-scale mean decreases in DO and pH were rare at 7 m water depth but were observed during Fall 2010 and 2011 (Table 2). In 2010, mean DO and pH dropped below $200\,\mu mol\,kg^{-1}$ and 7.9 units for an extended period of time on two occasions. The first event lasted for two days from 4–5 September 2010, and the end of the second event was not captured but lasted > 1.4 d. In 2011, mean DO dropped below $200\,\mu mol\,kg^{-1}$ four times (corresponding pH data not available). Each event lasted between one and five days.

Changes in DO and pH variability regimes: We have documented large daily ranges in pH and DO, with magnitudes corresponding to alongshore current direction. Daily DO and pH ranges were greatly enhanced when alongshore currents were equatorward (Fig. 4). As an example, between 29 September 2010–9 November 2010, DO and pH varied up to $113\,\mu mol\,kg^{-1}\,d^{-1}$ and $0.22\,units\,d^{-1}$, respectively. When

Table 1. Event-scale mean increases in dissolved oxygen (ΔDO) and pH (ΔpH) proceeding intrusion of high-density water ($\sigma > 25.1\,kg\,m^{-3}$) at 7 m water depth. v and u indicate the mean velocity ($cm\,s^{-1}$) of alongshore and cross-shore currents, respectively, between 5 and 30 m for 7 d before and after the event. Negative values are equatorward or offshore for v and u, respectively. Positive values of ΔDO and ΔpH indicate mean increases from before to after the event. Events are ordered by magnitude of ΔDO.

Event start	Mooring	v before	v after	u before	u after	ΔDO	ΔpH
14 Jul 2010	B	−1.6	4.3	0.5	1.0	66	0.07
26 Apr 2011	A	−3.8	10.9	0.7	2.5	63	0.10
26 Apr 2011	D	−3.8	10.9	0.7	2.5	62	0.10
27 Nov 2010	A	−4.4	5.9	1.2	0.8	35	0.03
31 Jul 2011	A	0.8	0.0	1.2	3.4	35	0.01
21 Aug 2010	A	0.3	4.2	−0.7	0.1	25	0.03
21 Aug 2010	B	0.3	4.2	−0.7	0.1	−2	−0.02

Table 2. Low dissolved oxygen (ΔDO) and pH (ΔpH) events at 7 m water depth at mooring A. Event start date is day that low-pass filtered DO and pH fell below $200\,\mu mol\,kg^{-1}$ and 7.9 units, respectively. nd = no data.

Event start	Duration	Mean DO	Mean pH	Mean density
04 Sep 2010	1.8	136	7.82	25.5
12 Sep 2010	> 1.4	167	7.88	25.0
03 Sep 2011	4.5	180	nd	25.0
21 Sep 2011	2.3	189	nd	25.0
01 Oct 2011	1.1	184	nd	25.0
16 Oct 2011	3.1	184	nd	25.0

alongshore currents were directed poleward, the maximum daily range in DO and pH was reduced to $40\,\mu mol\,kg^{-1}$ and 0.01 units, respectively.

3.2 Spatial variability in dissolved oxygen and pH

3.2.1 Changes in dissolved oxygen and pH with water depth

Simultaneous measurements at 7 and 17 m documented large differences in mean DO and pH over small depth scales within the kelp forest (Fig. 5). Mean DO and pH in shallow water were $259\,\mu mol\,kg^{-1}$ and 8.07, respectively. Only 10 m deeper, mean DO and pH were $168\,\mu mol\,kg^{-1}$ and 7.87. These represent a 35 % decrease and 37 % increase in DO and $[H^+]$, respectively, from 7 to 17 m. Deep DO and pH were below $130\,\mu mol\,kg^{-1}$ and 7.8 for 20 % of the time, and the minimum DO and pH observed were $86\,\mu mol\,kg^{-1}$ and 7.67, respectively. Over this 10 m depth range, the average DO and pH gradients were $9\,\mu mol\,kg^{-1}\,m^{-1}$ and $0.02\,pH\,units\,m^{-1}$. The large differences between the DO and pH environment were related to the strength of density stratification (Fig. 6a and b). When the water column was well-stratified, DO and pH decreased with increasing depth. A density difference of 0.2–1 $kg\,m^{-3}$ could

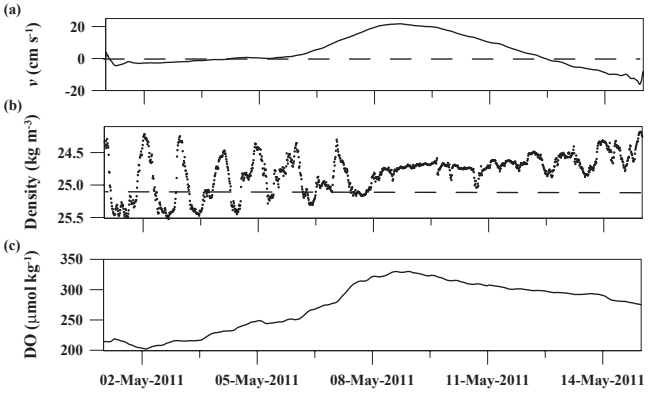

Fig. 3. Event-scale increases in dissolved oxygen (DO) following the intrusion of high-density seawater ($\sigma > 25.1\,kg\,m^{-3}$) at 7 m below the surface at mooring D. **(a)** Mean alongshore current velocity between 5 and 30 m at the Del Mar buoy, **(b)** time series of density and **(c)** time series of 2-d smoothed DO from 26 April 2011–16 May 2011. Density scale is reversed. Positive alongshore velocities indicate poleward flow.

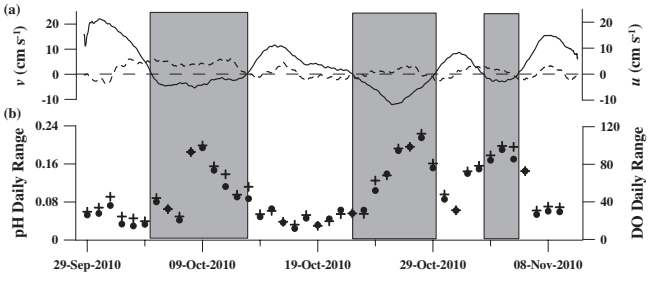

Fig. 4. (a) Mean alongshore current velocity (v: solid) and mean cross-shore current velocity (u: dotted) between 5 and 30 m from the Del Mar buoy and **(b)** daily range in pH (circles) and dissolved oxygen (DO: crosses) from mooring A at 7 m water depth. Grey-shaded rectangles indicate time periods when alongshore velocities are equatorward (negative). See Fig. 8 for corresponding time series of density, DO and pH.

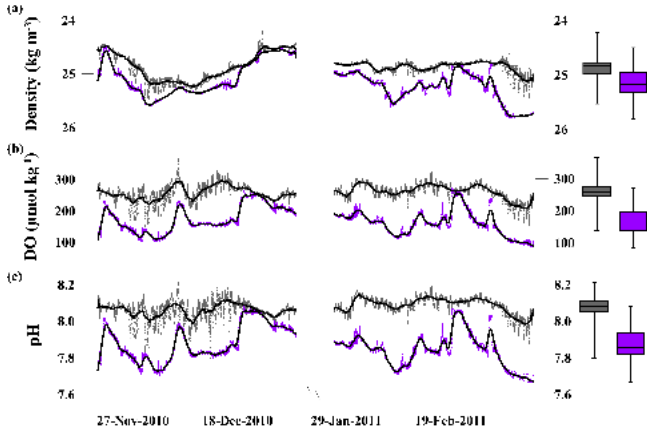

Fig. 5. Density, dissolved oxygen (DO) and pH comparisons between 7 m (grey) and 17 m (purple) at mooring A during two separate deployments. Time series and corresponding box plots of **(a)** density, **(b)** dissolved oxygen and **(c)** pH. Black solid lines are 2-d smoothed data. Density scale is reversed. Box plots at right depict the minimum, maximum, median, lower quartile and upper quartile for corresponding time-series data.

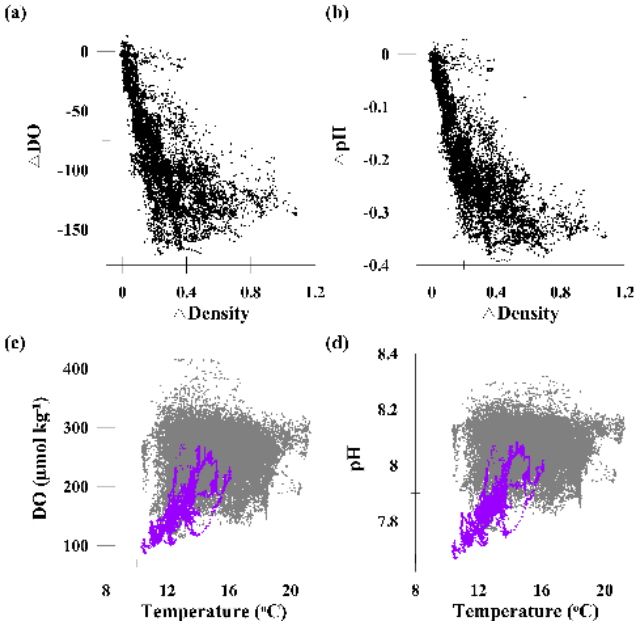

Fig. 6. Scatter plots of **(a)** density difference (ΔDensity) and dissolved oxygen difference (ΔDO) between 7 and 17 m at mooring A, and **(b)** ΔDensity and pH difference (ΔpH) between 7 and 17 m at mooring A. Includes all data from Fig. 5. Scatter plots of **(c)** temperature and DO, and **(d)** temperature and pH at 7 m (grey hatches) and 17 m (purple hatches) below the surface from all SeapHOx deployments from 10 July 2010–19 October 2011.

equate to a 0.4 unit decrease in pH and a DO reduction of 170 μmol kg^{-1}. On one occasion, starting on 19 December 2010, the water column was well-mixed, but on the fourth day DO and pH steadily decreased at 17 m while remaining stable near the surface; there was no apparent stratification between depths ($\sigma_{7\,m} \approx \sigma_{17\,m}$, Fig. 5). This suggests that the photosynthesis to respiration ratio ($P:R$) in deep water was below one. Variability patterns were also different in deep and shallow water. The mean change per hour in DO in shallow water was 4 μmol kg^{-1} h^{-1} (SD = 7.04), whereas in deep water the mean rate of change was 2.5 μmol kg^{-1} h^{-1} (SD = 4.43). In shallow water the mean change per hour in pH was 0.01 units h^{-1} (SD = 0.02); in deep water the mean rate of change was only 0.006 units h^{-1} (SD = 0.01). Thus, the near-surface DO and pH conditions were more variable on semidiurnal and diurnal timescales, while near-bottom depths (17 m; 3 mab) exhibited more stable conditions at high frequencies and large changes were associated with the structure of the water column over event time scales.

3.2.2 Alongshore changes in dissolved oxygen and pH within the kelp forest

Differences in DO and pH within the kelp forest were examined 5 km apart in an alongshore direction at 7 m water depth. The moorings were located in north and south LJKF. There were minimal but significant differences in DO and pH during the study period (Fig. 7). Mean DO was 258 versus 252 μmol kg^{-1} ($t = 5.8$, $d.f. = 2469$, $P < 0.001$) and mean pH was 8.10 versus 8.05 in north LJKF (mooring D) versus south LJKF (mooring A), respectively ($t = 17.5$, $d.f. = 2469$, $P < 0.001$). The average gradient from north to south in DO and pH were negligible (e.g., < 1.5 μmol kg^{-1} km^{-1} and 0.01 units km^{-1}). Temporal variability was also similar at both sites. Concordant high-frequency, large excursions in DO and pH occurred on diurnal and semidiurnal frequencies at both moorings. Event-scale increases in DO and pH resulting from biological production in response to the intrusion of high-density, high-nutrient seawater were observed in both the north and south LJKF, and magnitudes of change were very similar (Table 1; event start = 26 April 2011). This suggests that the spatial scale of these events can span the entire length of the kelp forest (≥ 5 km). However, beginning 16 May 2011 higher density waters, with a low pH and DO signature, were observed in south LJKF but not in north LJKF for two days. At that time, the gradient in DO and pH from south to north significantly increased to 20 μmol kg^{-1} km^{-1} and 0.05 units km^{-1}, respectively. Mean temperature was 1 °C cooler in south LJKF versus north LJKF. This discrepancy between north and south LJKF was also observed earlier in the month, between 1 May and 6 May 2011. Thus, in general there was a great deal of coherence in DO and pH in north and south LJKF but minor differences existed and were likely related to different local forcing dynamics.

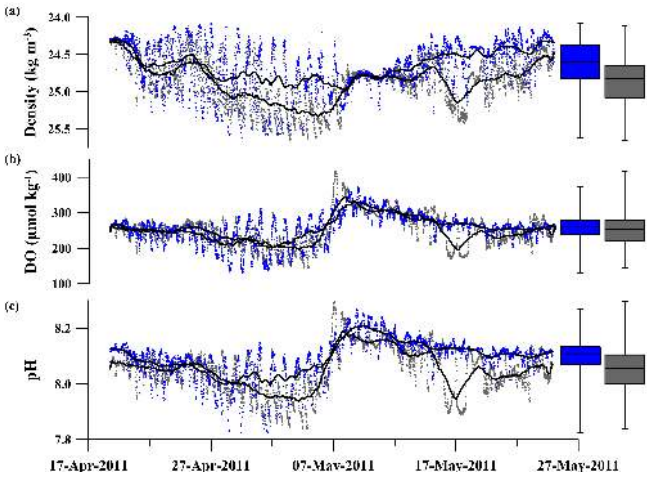

Fig. 7. Alongshore comparisons in density, dissolved oxygen (DO) and pH in the south and north La Jolla kelp forest. Time series and corresponding box plots of **(a)** density, **(b)** DO and **(c)** pH at south LJKF (mooring A; grey) and north LJKF (mooring D; blue) at 7 m below the surface. Black solid lines are 2-d smoothed data. Density scale is reversed. Box plot depicts the minimum, maximum, median, lower quartile and upper quartile for corresponding time-series data.

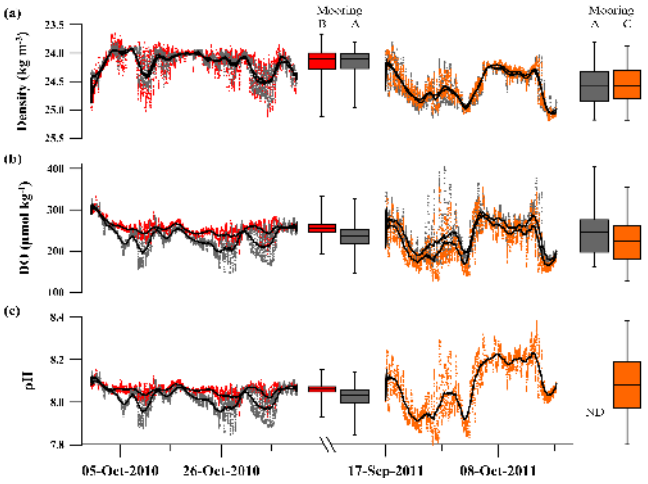

Fig. 8. Cross-shore differences in time series and corresponding box plots of **(a)** density, **(b)** dissolved oxygen (DO) and **(c)** pH. From 28 September 2010–10 November 2010, one SeapHOx was deployed at mooring B, 3.5 km from the coast (red), and the other SeapHOx was deployed at mooring A, 1.9 km from the coast (grey). From 26 September 2011–18 October 2011, one SeapHOx was deployed at mooring A, 1.9 km from the coast (grey), and the other SeapHOx was deployed at mooring C, 1.4 km from the coast (orange). Black solid lines are 2-d smoothed data. Density scale is reversed. Box plot depicts the minimum, maximum, median, lower quartile and upper quartile for corresponding time-series data. ND = no data.

3.2.3 Cross-shore changes in dissolved oxygen and pH on the inner shelf

DO and pH conditions varied strongly with proximity to shore. Mean DO and pH at 7 m decreased with decreasing distance from shore, suggesting that isopleths of DO and pH slope up towards the coast (Fig. 8). Two measurement experiments were conducted during the same months (September–November) in 2010 and 2011 along a zonal transect (Fig. 1). During 2010, mean DO was 20 µmol kg^{-1} lower at 1.9 km versus 3.5 km from the coast ($t = 37.3$, $d.f. = 4117$, $P < 0.001$), resulting in a DO gradient of -13 µmol kg^{-1} km^{-1} (towards the coastline). Mean pH was 0.03 units lower ($t = 38.5$, $d.f. = 4117$, $P < 0.001$), and the gradient was -0.02 units km^{-1}. These differences could not be attributed to water mass as the density gradient between moorings was negligible (< 0.01 kg m^{-3} km^{-1}), and there was no significant difference in density conditions ($P > 0.05$). The same trend emerged during 2011. Mean DO was 19 µmol kg^{-1} lower at 1.4 km versus 1.9 km from the coast ($t = 15.5$, $d.f. = 3064$, $P < 0.001$), and resulted in a gradient of -38 µmol kg^{-1} km^{-1}. A pH comparison was not available for 2011. Density was greater at the outer mooring ($t = 3.27$, $d.f. = 4117$, $P < 0.002$). The expectation would be that DO and pH would be greater closer to shore if considering only physical water excursion, but the opposite trend has emerged.

The decoupling between DO and pH with density was investigated by comparing the changes in the linear relationship between DO and pH with density with respect to distance from shore. At a given density, DO and pH were lower inshore relative to offshore, particularly at high density values. This phenomenon was corroborated by changes in the linear relationship between density and DO or pH with varying distance from shore. There was a significant decrease in the intercept of the linear relationship between density and DO with decreasing distance from shore during both years (2010: $t = 33.7$, $d.f. = 8231$, $P < 0.001$; 2011: $t = 14.2$, $d.f. = 6125$, $P < 0.001$). There was also a significant decrease in the intercept of the linear relationship between density and pH with decreasing distance from shore during 2010 ($t = 14.6$, $d.f. = 8231$, $P < 0.001$). These relationships illustrate that the change in the DO and pH environment with proximity to shore was due to shoaling isopleths that were decoupled from isopycnals.

3.3 Relationship between dissolved oxygen and pH

There was a significant, positive linear relationship between DO and pH for all data collected at 7 and 17 m water depths (pH = 0.002 × DO + 7.50, $R^2 = 0.96$, $P < 0.001$; Fig. 9). The linear relationship between DO and pH was more stable at depth than near the surface (7 m: $R^2 = 0.85$, $P < 0.001$; 17 m: $R^2 = 0.97$, $P < 0.001$), and the strong relationship between DO and pH indicates a mechanistic link. There were no significant linear relationships between DO or pH and temperature at 7 m water depth ($P > 0.05$;

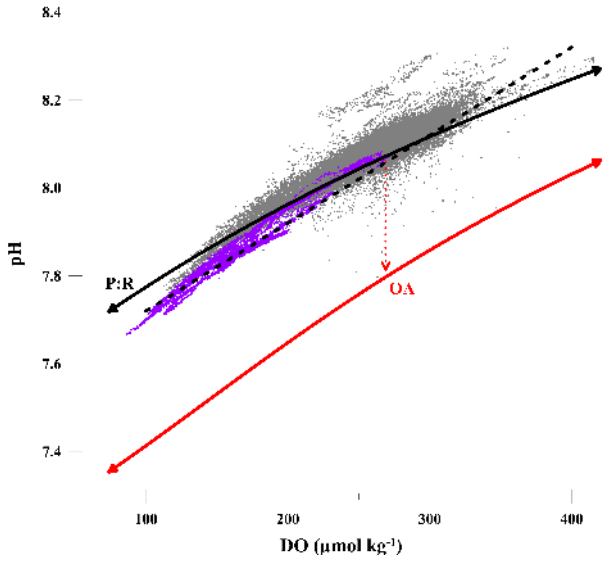

Fig. 9. Scatter plot of dissolved oxygen (DO) and pH at 7 m (grey hatches) and 17 m (purple hatches) water depth from all SeapHOx deployments from 10 July 2010–19 October 2011. Dashed black line is the linear relationship between pH and DO for all data regardless of depth. Solid black line represents expected changes in DO and pH with production and respiration ($P:R$) at present-day conditions (384 ppm CO_2). Future changes in pH due to ocean acidification are modeled at oxygen saturation and CO_2 levels of 800 ppm (OA; dashed red line) along with the corresponding changes in the $P:R$ relationship (solid red line).

Fig. 6c and d), but at 17 m there were positive linear relationships ($DO = 32.9 \times temp - 2.6$, $R^2 = 0.62$, $P < 0.001$; $pH = 0.08 \times temp + 6.88$, $R^2 = 0.67$, $P < 0.001$). The positive relationship between temperature and DO or pH can be best explained by biologically-driven gradients and is opposite to thermodynamically-predicted changes in temperature with DO or pH. The stronger correlation at depth suggests that physically forced changes via water movement are more important in driving changes in DO and pH in deeper waters, while local biochemical processes and air–sea gas exchange dominate at the surface.

Low DO and pH were linked, but high DO and pH were not. The minimum pH and DO values during this study were observed simultaneously at 17 m water depth on 30 December 2010; these were 7.67 and 86 µmol kg^{-1} (31 % saturation), respectively. The maximum pH value observed was 8.38 at 7 m water depth on 15 October 2011, whereas the maximum DO value observed was 415 µmol kg^{-1} (165 % saturation) at 7 m water depth on 7 May 2011. These findings indicate that low DO and pH are persistently linked in the LJKF benthic environment.

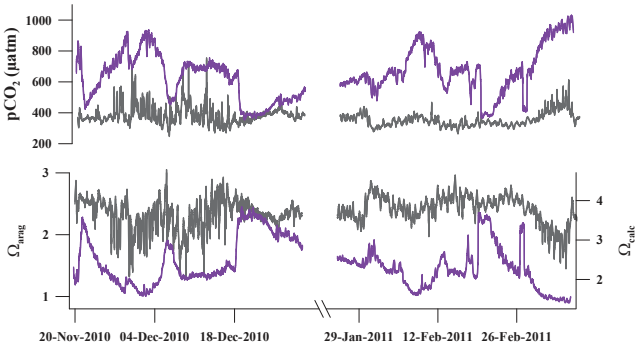

Fig. 10. Estimates of pCO_2 and saturation state of aragonite and calcite (Ω_{arag} and Ω_{calc}) at 7 m (grey) and 17 m (purple) water depth at mooring A during two separate deployments. The width of the line at each point represents the range estimated for pCO_2 or Ω as calculated from pH, temperature, and salinity measured by the SeapHOx sensor and a TA range of 2225–2260 µmol kg^{-1}.

3.4 Estimates of pCO_2 and saturation state in the LJKF

pCO_2, Ω_{arag}, and Ω_{calc} were estimated using sensor data collected at 7 m and 17 m during the depth experiment (data used corresponds with Fig. 5) along with TA ranges specific to this system. At 7 m water depth, estimated pCO_2 ranged between 246 and 820 µatm, and between 353 and 1016 µatm at 17 m water depth (Fig. 10). Estimated Ω_{arag} ranged between 1.15 and 3.05 at 7 m water depths, and between 0.90 and 2.45 at 17 m water depth (Fig. 10). Estimated Ω_{calc} ranged between 1.81 and 4.78 at 7 m water depth, and between 1.41 and 3.83 at 17 m water depth (Fig. 10). The highest pCO_2 and lowest Ω corresponded with the lowest DO and pH conditions observed.

4 Discussion

4.1 Temporal scales of dissolved oxygen and pH variability

Large ranges in DO and pH were observed on semidiurnal, diurnal and event time scales in the LJKF. This is not unexpected given that short-term fluctuations in many nearshore environments, including the California inner shelf, have been previously documented for many variables including temperature, nutrients, pH and DO (Kaplan et al., 2003; McPhee-Shaw et al., 2007; Moore et al., 2009; Jiang et al., 2011; Hofmann et al., 2011b; Booth et al., 2012). These dynamics are likely to be representative of all nearshore environments that are under strong influence of winds, tides, and upwelling, such as the major eastern boundary current (Benguela, California, Canary, Humboldt Current) systems. We expected to observe a prominent diel signal from production and respiration of the kelp forest ecosystem as has been observed in other kelp forests (Delille et al., 2009), but diel modulations

of DO and pH were not the dominant forcing observed in the LJKF. This could be due to strong water advection that may dampen the productivity signal by continually replenishing kelp forest waters, or the signal could have been counteracted by strong modulations from temperature. Diurnal changes in cross-shore advection can easily dominate in this study area due to intermittently enhanced diurnal winds associated with diurnal land–sea breeze (Pidgeon and Winant, 2005), wind- and tide-driven diurnal waves (Lerczak et al., 2001; Nam and Send, 2011), and sea/land breeze-driven resonant oscillations (Nam and Send, 2012).

The observed strong modulations of diurnal DO and pH fluctuations under equatorward currents (Fig. 4) are consistent with previous studies on the concentration and trapping of near-inertial (close to diurnal frequency in study location) internal wave energy under upwelling rather than downwelling conditions (Federiuk and Allen, 1996; Chant, 2001; Lerczak et al., 2001). Such internal waves are a primary mechanism supplying nitrate to kelp forests (McPhee-Shaw et al., 2007), and are important for sustaining kelp growth. During this study, kelp forest ecosystem production in response to high-density, high-nutrient seawater led to elevated DO and pH on event time scales encompassing a few days to weeks; mean increases in DO and pH were related to alongshore current direction and velocity (Fig. 4, Table 1). Poleward flow following upwelling advects low DO (and low pH) water along the shelf and results in event-scale DO and pH changes that can be as significant as the effects of isopycnal shoaling on DO and pH (Send and Nam, 2012). Our observations provide additional evidence for the significant role of alongshore currents in event-scale DO and pH variability. In particular, biological production is expected to regulate mean DO and pH conditions for weeks at a time. High-density waters were present while alongshore current direction was equatorward. The transition from strong equatorward to poleward currents corresponded with the accumulation of DO, and uptake of CO_2, yielding increases in pH. Ecosystem production in response to the intrusion of high-density waters to shallow depths was evident in the DO and pH records at multiple times throughout the year (Table 1).

4.2 Spatial scales of dissolved oxygen and pH variability

The largest gradients in DO and pH in this study occurred with changes in water depth. pH values not expected until 2100 at the surface in open ocean settings were observed frequently at 17 m depth in the LJKF (Caldeira and Wickett, 2003). The structure of the DO and pH gradient with depth was linked to the density structure of the water column, and so future changes in stratification will alter the duration and frequency over which benthic communities are exposed to low DO and pH conditions.

Cross-shore gradients in DO and pH were greater than alongshore gradients. These results correspond to previously documented long alongshore correlation scales in currents (Winant, 1983; Lentz and Winant, 1986), water properties, and nutrients (McPhee-Shaw et al., 2007). This suggests that fewer time series stations are needed in an alongshore direction relative to the cross-shore direction to accurately describe DO and pH dynamics.

DO and pH conditions at a given density decreased with decreasing distance from the shore. Mechanisms driving the cross-shore discrepancy among density, DO and pH warrant further investigation. The relationship between DO and pH was maintained at various distances from shore, but DO and pH decreased at a given density towards the shore. Anomalies in the DO and density relationships have been previously observed on the San Diego margin. DO and pH isopleths shoaled towards the coast at a greater rate than isopycnals. The mechanisms that explained the DO anomaly at the Del Mar buoy included decreased subsurface primary production and strengthened poleward flows by the California Undercurrent (Nam et al., 2011), yet the extent to which these processes account for the nearshore anomalies in density with DO or pH observed during this study in the LJKF is unknown. The greatest cross-shore gradients in DO and pH were observed during 2011. The observations were made further inshore (15 and 20 m bottom depth) than during 2010 (20 and 30 m bottom depth). At shallower bottom depths, benthic respiration may play a greater role in shoaling isopleths because benthic respiration processes are integrated over a smaller volume of water.

4.3 Relationship between dissolved oxygen and pH

The linear relationship between DO and pH was stable and coherent with depth, alongshore, and cross-shore directions in the context of this study (Fig. 9). The relationship was stronger with depth, and at high DO and high pH values there was nonlinearity. This nonlinearity may be explained by the expected changes in DO and pH with biological production and respiration ($P : R$) (Fig. 9), which are nonlinear. At high values of DO and pH, production generates a greater increase in DO than pH. The $P : R$ model was produced with mean temperature (14.8 °C), TA (2240 µmol kg^{-1}), and salinity (33.4) conditions. It assumes an $O_2 : CO_2$ Redfield ratio of $-150 : 106$ and a $TA : CO_2$ ratio of $-18 : 106$. The overlap of the $P : R$ model with the DO and pH relationship indicates that the biochemical consumption and production of O_2 is primarily responsible for the corresponding changes in DO and pH observed in the LJKF, and that calcification and dissolution of calcium carbonate play a more minor role. The $P : R$ model was then run under future atmospheric CO_2 conditions at 800 ppm (year 2100) using the same alkalinity, salinity, and temperature conditions but with an increase in DIC (+112 µmol kg^{-1}) at oxygen saturation. This model attributes all of the change in pH to anthropogenic CO_2 intrusion. At DO saturation, pH is expected to decrease by 0.20 units, while at low DO values, pH could be as low as 7.35, a decrease of 0.37 pH units from present low pH

conditions. The additional drop in pH at low DO is a consequence of the nonlinear nature of the carbonate system (Cai et al., 2011; Melzner et al., 2012). Nearshore CO_2-enriched habitats are expected to experience greater changes in pCO_2 than the open surface ocean and have been suggested to be particularly vulnerable habitats in a changing ocean climate (Brewer and Peltzer, 2009; Thomsen et al., 2010; Cai et al., 2011).

There was no significant linear relationship between temperature and DO or pH at shallow depths in contrast to the firm relationship at deeper depths in the region (e.g., Figs. 6c, d and S1 in Nam et al., 2011). DO and pH are more affected by biochemical processes at shallow versus deep depths, and these processes may account for the large deviations in the relationships between temperature and DO or pH.

4.4 Estimates of pCO_2 and saturation state in the LJKF

Increasing evidence suggests that species responses to ocean acidification vary for different carbonate system constituents (Fabry et al., 2008; Doney et al., 2009). Thus, full constraint of the carbonate system, beyond just pH measurements, is critical for defining this nearshore system and the potential sensitivity or resilience of its residents to ocean acidification. The observed range in TA in the LJKF ($35\,\mu mol\,kg^{-1}$) has relatively little influence on variability in pCO_2 in this system; instead, changes in pCO_2 are driven by large DIC gradients. Ω_{arag} was undersaturated at 17 m for a short period of time at the end of February and early March 2011. This also corresponded with the lowest DO concentrations observed (Fig. 5). While emphasis has been placed on the strong relationship between DO and pH, low DO also corresponds with low Ω_{arag}, low Ω_{calc}, and high pCO_2.

4.5 Biological implications of dissolved oxygen and pH trends

pH and DO in the LJKF vary on multiple timescales with large ranges; biological responses to pH and DO also unfold over a range of timescales. Rapid pH and DO changes can disturb an organism's extracellular and intracellular acid–base balance; in the LJKF these changes can be as great as $62\,\mu mol\,O_2\,kg^{-1}\,h^{-1}$ and 0.16 pH units h^{-1}. Different taxa react differently to these rapid excursions. For example, mussels cannot control extracellular pH (Thomsen et al., 2010), sea urchins take several days to adjust (Stumpp et al., 2012), and many fish and decapod crustaceans are able to rapidly regulate extracellular and intracellular pH (Heisler, 1984). The biological significance of these low values of DO and pH observed at 17 m water depth in the LJKF is unknown. However, these low values of DO ($< 90\,\mu mol\,kg^{-1}$) are considered to be sublethal thresholds for coastal species of fishes, crustaceans, and bivalves (Vaquer-Sunyer and Duarte, 2008). These groups are common and diverse within the kelp forest at depths deeper than 17 m where even lower DO concentrations occur (Parnell et al., 2006).

It is unclear which aspect of the DO and carbonate chemistry signals will shape ecological patterns and how these aspects are changing over time. Changes in the extremes, ranges, or patterns of variability need to be considered in the context of organismal sensitivity. Knowledge of DO thresholds and responses to low DO events by shelf animals in this region is limited and in need of further study, while our present understanding of organism and ecosystem sensitivity to carbonate chemistry is in relation to mean conditions. Laboratory studies have revealed that some species that are found within this study region, and particularly their early life stages, are sensitive to the pH values observed in and around the LJKF during this study at 17 m. For example, larvae of the mussel *Mytilus californianus*, a foundation species common on rocky shorelines in our study region, precipitated weaker, thinner, and smaller shells and had lower tissue mass at pH_{tot} values of 7.83 and 7.63 versus 7.95 (Gaylord et al., 2011; pH values converted from the National Bureau of Standards (NBS) scale to total scale at 15 °C). pH was observed below 7.83 in the LJKF in deeper waters 32 % of the time. Thus, it is possible that *M. californianus* larvae are exposed to pH conditions in the present day that may elicit laboratory-observed biological responses to low pH. Also, the echinoplutei of the sea urchin *Lytechinus pictus* were smaller and had altered gene expression in pH_{tot} treatments of 7.75 and 7.66 versus control conditions of 7.81 (O'Donnell et al., 2010; pH values converted from NBS to total scale at 18.5 °C). pH conditions less than 7.75 were observed 10 % of the time in the LJKF at 17 m water depth. These examples highlight the potential importance of vertical positioning for invertebrate larvae developing within the kelp forest. Another study on a resident urchin, *Strongylocentrotus franciscanus*, investigated the potential for evolutionary response in larval development to ocean acidification, and found that *S. franciscanus* larvae were smaller but that phenotypic and genetic variation could allow evolutionary responses within 50 yr in response to a pH decrease of 0.31–0.33 units (Sunday et al., 2011). Full understanding of implications will require integration of DO and pH dynamics with research on how oxygen and pH influence energetics, calcification, sinking and swimming behavior.

Our $P : R$ model predicts that under future scenarios of ocean acidification pH could be as low as 7.35 (corresponding pCO_2 of approximately 2100 µatm) at low DO concentrations. This drop could mean that carbonate chemistry will play a larger role in structuring marine ecosystems than DO if DO conditions remain the same over this time period. Yet, while pH may reach extreme low levels, the variability associated with these mean changes is unknown. When just considering changes in the pH and oxygen relationship due to ocean acidification, high-frequency in pH variability would increase relative to present-day variability. This is because in this system, changes in pH are largely driven by changes

in DIC. The same change in DIC at high concentrations will produce a greater change in pH than at low concentrations of DIC.

Still, there are many other processes that may change over the coming decades that will structure pH and oxygen dynamics. These include changes in water-column stability, the $P : R$ ratio, upwelling dynamics (e.g., timing and intensity), wind patterns, and the sources and chemical properties of water that are advected horizontally and vertically into upwelling margins. Model simulations of the California Current System indicate that the seafloor (50–120 m) will become exposed to year-round aragonite undersaturation by 2050 (Gruber et al., 2012). Additionally, future changes in upwelling dynamics in the SCB remain a critical topic for further research. Evidence suggests a general intensification of wind-driven coastal upwelling in major upwelling regions as greenhouse gas concentrations increase (Bakun et al., 2010; Narayan et al., 2010). These results suggest that DO could reach hypoxic values at increasingly shallower depths and result in habitat compression (or expansion) for intolerant (or tolerant) species. We suggest that in eastern boundary current systems biological sensitivity to changes in DO and pH will largely derive from changes that carry low DO and pH waters from depth into nearshore benthic habitats (Feely et al., 2008; Gruber, 2011; Hofmann et al., 2011a).

5 Conclusions

In this study, we show that DO and pH in an eastern Pacific kelp forest can be highly variable, tightly correlated, and reflect influences from many different processes including alongshore-current direction, internal tidal dynamics, and biological production. All of these features invoked large ranges in DO and pH, as well as in pCO_2, Ω_{arag}, and Ω_{calc}. The most extreme and consistent temporal scales of variation in DO and pH were semidiurnal and diurnal. The high productivity of the kelp forest can increase DO and pH on event time scales in response to nutrient-replete water intrusion. This phenomenon may serve to alleviate biological stress following low DO and pH events. Thus, kelp forests and similar macrophyte regions might provide temporary refugia from acidification and deoxygenation when high levels of productivity elevate DO and pH values relative to surrounding waters. The spatial distribution of DO and pH in the LJKF was largely uniform in an alongshore direction, there were minor differences in the cross-shore direction, and there were drastic depth effects that are largely related to stratification of the water column. Future changes in warming and upwelling in the SCB will have implications for the exposure, duration, and frequency of low DO and pH experienced by benthic species and their early life stages. It is likely that nearshore communities along eastern boundary current systems are preadapted to the range of pH and DO observed during this study. However, communities may respond to rapid transitions at sharply defined critical thresholds rather than experience an extended transition to decreased pH. There is a need for more continuous monitoring of DO and pH along with relevant corresponding physical and biochemical variables, particularly where hypoxia lies near the shelf (Hofmann et al., 2011a). Such data will facilitate a mechanistic understanding of DO and pH trends in highly variable and potentially vulnerable coastal ecosystems.

Acknowledgements. We would like to acknowledge B. Peterson and Y. Takeshita, who provided assistance with SeapHOx development and maintenance. We thank Andrew Dickson for providing access to his laboratory facilities to run DIC and TA samples. The ADCP data collected from the DM Buoy were provided by Uwe Send and the SIO Ocean Time Series Group (http://mooring.ucsd.edu). We thank all those who assisted with field and diving support, especially P. Zerofski, M. Navarro and G. Cook. We thank D. Holway, J. Leichter, and A. Dickson for comments on earlier drafts of this manuscript, and F. Melzner and an anonymous reviewer for helpful comments on the submitted manuscripts. This research was supported by NSF-OCE Award Nos. 0927445 and 1041062. This publication was developed under a Science to Achieve Results (STAR) Fellowship Assistance Agreement No. FP916973 awarded by the US Environmental Protection Agency (EPA). It has not been formally reviewed by the EPA. The views expressed in this publication are solely those of the authors.

Edited by: L. C. da Cunha

References

Alin, S. R., Feely, R. A., Dickson, A. G., Hernández-Ayón, J. M., Juranek, L. W., Ohman, M. D., and Goericke, R.: Robust empirical relationships for estimating the carbonate system in the southern California System and application to CalCOFI hydrographic cruise data (2005–2011), J. Geophys. Res., 117, C05033, doi:10,1029/2011JC007511, 2012.

Bakun, A., Field, D. B., Redondo-Rodriguez, A., and Weeks, S. J.: Greenhouse gas, upwelling-favorable winds, and the future of coastal ocean upwelling ecosystems, Glob. Change Biol., 16, 1213–1228, doi:10.1111/j.1365-2486.2009.02094.x, 2010.

Bograd, S. J., Castro, C. G., Di Lorenzo, E., Palacios, D. M., Bailey, H., Gilly, W., and Chavez, F. P.: Oxygen declines and the shoaling of the hypoxic boundary in the California Current, Geophys. Res. Lett., 35, L12607, doi:10.1029/2008GL034185, 2008.

Booth, J. A. T., McPhee-Shaw, E. E., Chua, P., Kingsley, E., Denny, M., Phillips, R., Bograd, S. J., Zeidberg, L. D., and Gilly, W. F.: Natural intrusions of hypoxic, low pH water into nearshore marine environments on the California coast, Cont. Shelf Res., 45, 108–115, doi:10.1016/j.csr.2012.06.009, 2012.

Bray, N. A., Keyes, A., and Morawitz, W. M. L.: The California Current system in the Southern California Bight and the Santa Barbara Channel, J. Geophys. Res., 104, 7695–7714, 1999.

Brewer, P. G. and Peltzer, E. T.: Limits to marine life, Science, 324, 347–348, doi:10.1126/science.1170756, 2009.

Cai, W.-J., Hu, X., Huang, W.-J., Murrell, M. C., Lehrter, J. C., Lohrenz, S. E., Chou W.-C., Zhai, W., Hollibaugh, J. T., Wang, Y., Zhao, P., Guo, X., Gundersen, K., Dai, M., and Gong, G.-C.: Acidification of subsurface coastal waters enhance by eutrophication, Nat. Geosci., 4, 766–770, doi:10.1038/NGEO1297, 2011.

Caldeira, K. and Wickett, M. E.: Anthropogenic carbon and ocean pH, Nature, 425, p. 365, 2003.

Chant, R. J.: Evolution of near-inertial waves during an upwelling event on the New Jersey inner shelf, J. Phys. Oceanogr., 31, 746–764, 2001.

Connell, S. D. and Russell, B. D.: The direct effects of increasing CO_2 and temperature on non-calcifying organisms: increasing the potential for phase shifts in kelp forests, P. R. Soc. B, 277, 1409–1415, doi:10.1098/rspb.2009.2069, 2010.

Cullison Gray, S. E., DeGrandpre, M. D., Moore, T. S., Martz, T. R., Friederich, G. E., and Johnson, K. S.: Application of *in situ* pH measurements for inorganic carbon calculations, Mar. Chem., 125, 82–90, 2011.

Delille, B., Borges, A. V., and Delille, D.: Influence of giant kelp beds (*Macrocystis pyrifera*) on diel cycles of pCO_2 and DIC in the Sub-Antarctic coastal area, Estuar. Coast. Shelf S., 81, 114–122, 2009.

Dickson, A. G. and Millero, F. J.: A comparison of the equilibrium constants for the dissociation of carbonic acid in seawater media, Deep-Sea Res., 34, 1733–1743, 1987.

Dickson, A. G., Sabine, C. L., and Christian, J. R.: Guide to best practices for ocean CO_2 measurements, Vol. 3, 374 PICES Spec. Publ., Sidney, British Columbia, 2007.

Doney, S. C., Fabry, V. J., Feely, R. A., and Kleypas, J. A.: Ocean acidification: The other CO_2 problem, Annu. Rev. Mar. Sci., 1, 169–192, doi:10.1146/annurev.marine.010908.163834, 2009.

Doney, S. C., Ruckelshaus, M., Duffy, J. E., Barry, J. P., Chan, F., English, C. A., Galindo, H. M., Grebmeier, J. M., Hollowed, A. B., Knowlton, N., Polovina, J., Rabalais, N. N., Sydeman, W. J., and Talley, L. D.: Climate change impacts on marine ecosystems, Annu. Rev. Mar. Sci., 4, 11–37, doi:10.1146/annurev-marine-041911-111611, 2012.

Dong, C., Idica, E. Y., and McWilliams, J. C.: Circulation and multiple-scale variability in the Southern California Bight, Prog. Oceanogr., 82, 168–190, 2009.

Fabry, V. J., Seibel, B. A., Feely, R. A., and Orr, J. C.: Impacts of ocean acidification on marine fauna and ecosystem processes, ICES J. Mar. Sci., 65, 414–432, 2008.

Federiuk, J. and Allen, J. S.: Model studies of near-inertial waves in flow over the Oregon continental shelf, J. Phys. Oceanogr., 26, 2053–2075, 1996.

Feely, R. A., Sabine, C. L., Hernandez-Ayon, J. M., Ianson, D., and Hales, B.: Evidence for upwelling of corrosive "acidified" water onto the continental shelf, Science, 320, 1490–1492, doi:10.1126/science.1155676, 2008.

Gaylord, B., Hill, T. M., Sanford, E., Lenz, E. A., Jacobs, L. A., Sato, K. N., Russel A. D., and Hettinger, A.: Functional impacts of ocean acidification in an ecologically critical foundation species, J. Exp. Biol., 214, 2586–2594, 2011.

Graham, M. H., Vásquez, J. A., and Buschmann, A. H.: Global ecology of the giant kelp *Macrocystis*: From ecotypes to ecosystems, Oceanogr. Mar. Biol., 45, 39–88, 2007.

Gruber, N.: Warming up, turning sour, losing breath: ocean biogeochemistry under global change, Phil. T. R. Soc. A, 369, 1980–1996, doi:10.1098/rsta.2011.0003, 2011.

Gruber, N., Hauri, C., Lachkar, Z., Loher, D., Frölicher, T. L., and Plattner, G.-K.: Rapid progression of ocean acidification in the California Current System, Science, 337, 220–223, 2012.

Harley, C. D. G., Anderson, K. M., Demes, K. W., Jorve, J. P., Kordas, R. L., and Coyle, T. A.: Effects of climate change on global seaweed communities, J. Phycol., 48, 1064–1078, doi:10.1111/j.1529-8817.2012.01224.x, 2012.

Heisler, N.: Acid-base regulation in fishes, in: Fish Physiology, vol. X, edited by: Hoar, W. S. and Randall D. J., 315–401, San Diego: Academic Press, 1984.

Hepburn, C. D., Pritchard, D. W., Cornwall, C. E., McLeod, R. J., Beardall, J., Raven, J. A., and Hurd, C. L.: Diversity of carbon use strategies in a kelp forest community: Implications for a high CO_2 ocean, Glob. Change Biol., 17, 2488–2497, doi:10.1111/j.1365-2486.2011.02411.x, 2011.

Hofmann, A. F., Peltzer, E. T., Walz, P. M., and Brewer, P. G.: Hypoxia by degrees: Establishing definitions for a changing ocean. Deep-Sea Res. Pt. I, 58, 1212–1226, doi:10.1016/j.dsr.2011.09.004, 2011a.

Hofmann, G. E., Smith, J. E., Johnson, K. S., Send, U., Levin, L. A., Micheli, F., Paytan, A., Price, N. N., Peterson B., Takeshita, Y., Matson, P. G., Crook, E. D., Kroeker, K. J., Gambi, M. C., Rivest, E. B., Frieder, C. A., Yu, P. C., and Martz, T. R.: High-frequency dynamics of ocean pH: A multi-ecosystem comparison, PLoSONE, 6, e28983, doi:10.1371/journal.pone.0028983, 2011b.

Jiang, Z.-P., Huang, J.-C., Dai, M., Kai, S. J., Hydes, D. J., Chou, W.-C., and Jan, S.: Short-term dynamics of oxygen and carbon in productive nearshore shallow water systems off Taiwan: Observations and modeling, Limnol. Oceanogr., 56, 1832–1849, 2011.

Kaplan, D. M., Largier, J. L., Navarrete, S., Guiñez, R., and Castilla, J. C.: Large diurnal temperature fluctuations in the nearshore water column, Estuar. Coast. Shelf S., 57, 385–398, 2003.

Keeling, R. F., Körtzinger, A., and Gruber, N.: Ocean deoxygenation in a warming world, Annu. Rev. Mar. Sci., 2, 199–229, doi:10.1146/annurev.marine.010908.163855, 2010.

Lentz, S. J. and Winant, C. J.: Subinertial currents on the Southern California shelf, J. Phys. Oceanogr., 16, 1737–1749, 1986.

Lerczak, J. A., Hendershott, M. C., and Winant, C. D.: Observations and modeling of coastal internal waves driven by a diurnal sea breeze, J. Geophys. Res., 106, 19715–19729, 2001.

Lluch-Cota, D. B., Wooster, W. S., and Hare, S. R.: Sea surface temperature variability in coastal areas of the northern Pacific related to the El Niño-Southern Oscillation and Pacific Decadal Oscillation, Geophys. Res. Lett., 28, 2029–2032, doi:10.1029/2000GL012429, 2001.

Martz, T. R., Connery, J. G., and Johnson, K. S.: Testing the Honeywell Durafet® for seawater pH applications, Limnol. Oceanogr.-Meth., 8, 172–184, 2010.

McClatchie, S., Goericke, R., Cosgrove, R., Auad, G., and Vetter, R.: Oxygen in the Southern California Bight: Multidecadal trends and implications for demersal fisheries, Geohpys. Res. Lett., 37, L19602, doi:10.1029/2010GL044497, 2010.

McPhee-Shaw, E. E., Siegel, D. A., Washburn, L., Brzezinski, M. A., Jones, J. L., Leydecker, A., and Melack, J.: Mechanisms for nutrient delivery to the inner shelf: Observations from the Santa Barbara Channel, Limnol. Oceanogr., 52, 1748–1766, 2007.

Mehrbach, C., Culberson, C. H., Hawley, J. E., and Pytkowicz, R. N: Measurement of the apparent dissociation constants of carbonic acid in seawater at atmospheric pressure, Limnol. Oceanogr., 18, 897–907, 1973.

Melzner, F., Thomsen, J., Koeve, W., Oschlies, A., Gutowska, M. A., Bange, H. W., Hansen, H. P., and Körtzinger, A.: Future ocean acidification will be amplified by hypoxia in coastal habitats, Mar. Biol., doi:10.1007/s00227-012-1954-1, in press, 2012.

Moore, T. S., Nuzzio, D. B., Di Toro, D. M., and Luther III, G. W.: Oxygen dynamics in a well mixed estuary, the lower Deleware Bay, USA, Mar. Chem., 117, 11–20, 2009.

Nam, S. and Send, U.: Direct evidence of deep-water intrusions onto the continental shelf via surging internal tides, J. Geophys. Res., 116, C05004, doi:10.1029/2010JC006692, 2011.

Nam, S. and Send, U.: Resonant diurnal oscillations and mean alongshore flows driven by sea/land breeze forcing in the coastal Southern California Bight, J. Phys. Oceanogr., in revision, 2012.

Nam, S., Kim, H.-J., and Send, U.: Amplification of hypoxic and acidic events by La Niña conditions on the continental shelf off California, Geophys. Res. Lett., 38, L22602, doi:10.1029/2011GL049549, 2011.

Narayan, N., Paul, A., Mulitza, S., and Schulz, M.: Trends in coastal upwelling intensity during the late 20th century, Ocean Sci., 6, 815–823, doi:10.5194/os-6-815-2010, 2010.

North, W. J., James, D. E., and Jones, L. G.: History of kelp beds (*Macrocystis*) in Orange and San Diego Counties, California, Hydrobiologia, 260/261, 277–283, 1993.

O'Donnell, M. J., Todgham, A. E., Sewell, M. A., Hammond, L. M., Ruggiero, K., Fangue, N. A., Zippay, M. L., and Hofmann, G. E.: Ocean acidification alters skeletogenesis and gene expression in larval sea urchins, Mar. Ecol.-Prog. Ser., 398, 157–171, 2010.

Parnell, P. E., Dayton, P. K., Lennert-Cody, C., Rasmussen, L. L., and Leichter, J. J.: Marine reserve design: Optimal size, habitats, species affinities, diversity, and ocean microclimate, Ecol. Appl., 16, 945–962, 2006.

Parnell, P. E., Miller, E. F., Lennert-Cody, C. E., Dayton, P. K., Carter, M. L., and Stebbins, T. D.: The response of giant kelp (*Macrocystis pyrifera*) in southern California to low-frequency climate forcing, Limnol. Oceanogr., 55, 2686–2702, 2010.

Pidgeon, E. J. and Winant, C. D.: Diurnal variability in currents and temperature on the continental shelf between central and southern California, J. Geophys. Res., 110, C03024, doi:10.1029/2004JC002321, 2005.

Pineda, J.: Circulation and larval distribution in internal tidal bore warm fronts, Limnol. Oceanogr., 44, 1400–1414, 1999.

Pringle, J. M. and Riser, K.: Remotely forced nearshore upwelling in Southern California, J. Geophys. Res., 108, 3131, doi:10.1029/2002JC001447, 2003.

Roleda, M. Y., Morris J. N., McGraw, C. M., and Hurd C. L.: Ocean acidification and seaweed reproduction: increased CO_2 ameliorates the negative effect of lowered pH on meiospore germination in the giant kelp *Macrocystis pyrifera* (Laminariales, Phaeophyceae), Glob. Change Biol., 18, 854–864, doi:10.1111/j.1365-2486.2011.02594.x, 2012.

Send, U. and Nam, S.: Relaxation from upwelling: the effect on dissolved oxygen on the continental shelf, J. Geophys. Res., 117, C04024, doi:10.1029/2011JC007517, 2012.

Stummp, M., Trübenbach, K., Brennecke, D., Hu., M. Y., and Melzner F.: Resource allocation and extracellular acid-base status in the sea urchin *Strongylocentrotus droebachiensis* in response to CO_2 induced seawater acidification, Aquat. Toxicol. 110–111, 194–207, doi:10.1016/j.aquatox.2011.12.020, 2012.

Sunday, J. M., Crim, R. N., Harley, C. D. G., and Hart, M. W.: Quantifying rates of evolutionary adaptation in response to ocean acidification, PLoS ONE, 6, e22881, doi:10.1371/journal.pone.0022881, 2011.

Swanson, A. K. and Fox, C. H.: Altered kelp (Laminariales) phlorotannins and growth under elevated carbon dioxide and ultraviolet-B treatments can influence associated intertidal food webs, Glob. Change Biol., 13, 1696–1709, doi:10.1111/j.1365-2486.2007.01384.x, 2007.

Thomsen, J., Gutowska, M. A., Saphörster, J., Heinemann, A., Trübenbach, K., Fietzke, J., Hiebenthal, C., Eisenhauer, A., Körtzinger, A., Wahl, M., and Melzner, F.: Calcifying invertebrates succeed in a naturally CO_2-rich coastal habitat but are threatened by high levels of future acidification, Biogeosciences, 7, 3879–3891, doi:10.5194/bg-7-3879-2010, 2010.

van Heuven, S., Pierrot, D., Rae, J. W. B., Lewis, E., and Wallace, D. W. R.: MATLAB program developed for CO_2 system calculations, ORNL/CDIAC-105b, Carbon Dioxide Information Analysis Center, Oak Ridge National Laboratory, US Department of Energy, Oak Ridge, Tennessee, doi:10.3334/CDIAC/otg.CO2SYS_MATLAB_v1.1, 2011.

Vaquer-Sunyer, R. and Duarte, C. M.: Thresholds of hypoxia for marine biodiversity, P. Natl. Acad. Sci. USA, 105, 15452–15457, doi:10.1073/pnas.0803833105, 2008.

Winant, C. D.: Longshore coherence of currents on the Southern California Shelf during the summer, J. Phys. Oceanogr., 13, 55–64, 1983.

Yu, P. C., Matson, P. G., Martz, T. R., and Hofmann, G. E.: The ocean acidification seascape and its relationship to the performance of calcifying marine invertebrates: Laboratory experiments on the development of urchin larvae framed by environmentally-relevant pCO_2/pH, J. Exp. Mar. Biol. Ecol., 400, 288–295, doi:10.1016/j.jembe.2011.02.016, 2011.